Dark Light-Higgs Bosons

Patrick Draper, Tao Liu, Carlos E. M. Wagner, Lian-Tao Wang, and Hao Zhang

Phys. Rev. Lett. **106**, 121805 — Published 24 March 2011

DOI: 10.1103/PhysRevLett.106.121805

Dark Light Higgs

Patrick Draper,[1] Tao Liu,[1,2] Carlos E.M. Wagner,[1,3,4] Lian-Tao Wang,[5] and Hao Zhang[1,6]

[1]*Enrico Fermi Institute, University of Chicago, Chicago, IL 60637, USA*
[2]*Department of Physics, University of California, Santa Barbara, CA 93106, USA*
[3]*HEP Division, Argonne National Laboratory, 9700 Cass Ave., Argonne, IL 60439, USA*
[4]*KICP and Dept. of Physics, Univ. of Chicago, 5640 S. Ellis Ave., Chicago IL 60637, USA*
[5]*Department of Physics, Princeton University, Princeton, NJ 08540, USA*
[6]*Department of Physics and State Key Laboratory of Nuclear Physics and Technology, Peking University, Beijing 100871, China*

We study a limit of the nearly-Peccei-Quinn-symmetric Next-to-Minimal Supersymmetric Standard Model possessing novel Higgs and dark matter (DM) properties. In this scenario, there naturally co-exist three light singlet-like particles: a scalar, a pseudoscalar, and a singlino-like DM candidate, all with masses of order 0.1-10 GeV. The decay of a Standard Model-like Higgs boson to pairs of the light scalars or pseudoscalars is generically suppressed, avoiding constraints from collider searches for these channels. For a certain parameter window annihilation into the light pseudoscalar and exchange of the light scalar with nucleons allow the singlino to achieve the correct relic density and a large direct detection cross section consistent with the CoGeNT and DAMA/LIBRA preferred region simultaneously. This parameter space is consistent with experimental constraints from LEP, the Tevatron, Υ- and flavor physics.

The Next-to-Minimal Supersymmetric Standard Model (NMSSM) is a well-motivated extension of the Minimal Supersymmetric Standard Model (MSSM) by a gauge-singlet chiral superfield $\mathbf{N}$, designed to solve the μ-problem of the MSSM. Its superpotential and soft supersymmetry-breaking terms in the Higgs sector are

$$\begin{aligned}\mathbf{W} &= \lambda \mathbf{N}\mathbf{H_u}\mathbf{H_d} + \frac{1}{3}\kappa \mathbf{N}^3,\\ V_{soft} &= m_{H_d}^2|H_d|^2 + m_{H_u}^2|H_u|^2 + m_N^2|N|^2\\ &\quad - (\lambda A_\lambda H_u H_d N + h.c.) + \left(\frac{\kappa}{3}A_\kappa N^3 + h.c.\right). \quad (1)\end{aligned}$$

Here H_d, H_u and N denote the neutral Higgs bosons corresponding to $\mathbf{H_d}$, $\mathbf{H_u}$ and $\mathbf{N}$, respectively.

In this work, we examine an NMSSM limit given by two conditions. The first one is $\kappa \ll \lambda$ which is protected by an approximate Peccei-Quinn (PQ) symmetry. It is well-known that a light pseudoscalar a_1 will be generated by the spontaneous breaking of such a $U(1)$ symmetry (the phenomenology on a light a_1 has been thoroughly studied in the R-symmetry limit [1, 2]). As noted in [3], at tree level the PQ limit implies an upper bound on the lightest scalar mass m_{h_1} approximately proportional to λ^2. Here we address the further limit of $\lambda \lesssim 0.1$, leading to the simultaneous emergence of a light singlet-like scalar h_1 and a light singlino-like lightest superpartner χ_1. For mildly small values of λ ($\lambda > 0.05$) studied in this letter, typically $\lambda(\Lambda_{\rm GUT}) \sim \mathcal{O}(0.1)$, a natural order for a perturbative parameter. We stress that this scenario differs from the light a_1 case of [1, 2], in that h_1, a_1, and χ_1 are all of order $0.1 - 10$ GeV. It also differs in that decays of the Standard Model (SM)-like Higgs boson to h_1h_1 and a_1a_1 pairs are generically suppressed. Thus h_1 and a_1 are hidden from four-fermion searches at LEP [4] and the Tevatron [5] designed to test a light a_1 scenario. Meanwhile, due to annihilation into a_1 and exchange of h_1, for a certain window of the parameters, the correct relic density and a large spin-independent (SI) direct detection cross section consistent with the CoGeNT and DAMA/LIBRA preferred region can be achieved for the DM candidate χ_1. Therefore, we refer to this limit as the "Dark Light Higgs" (DLH) scenario.

We begin with an analysis of the light spectrum in the DLH scenario. For convenience we define two parameters

$$\varepsilon \equiv \frac{\lambda\mu}{m_Z}\varepsilon', \quad \varepsilon' \equiv \frac{A_\lambda}{\mu\tan\beta} - 1 \quad (2)$$

with $\mu \equiv \lambda\langle N\rangle$. ε has an impact on Higgs physics, as exhibited in FIG. 1. In the first column of FIG. 1 we plot m_{h_1,a_1,χ_1} against ε for a random scan as defined in the figure caption. NMSSMTools 2.3.1 and MicrOMEGAS 2.4.Q [6, 7] are our analysis tools used in this letter.

The scan results in FIG. 1 can be understood analytically as follows. Because of the spontaneous breaking of the approximate PQ symmetry, a_1 is a pseudo-Goldstone boson and its small mass $m_{a_1}^2 \approx -3\kappa A_\kappa\mu/\lambda$ is protected. For χ_1, $\kappa \ll \lambda \ll 1$ implies that it is dominantly singlino and its mass is $m_{\chi_1} \approx v^2\lambda^2\sin 2\beta/\mu + 2\kappa\mu/\lambda$, where $v = 174$ GeV and $\tan\beta \equiv \langle H_u\rangle/\langle H_d\rangle$. For $\lambda \lesssim 0.1$, μ of order a few hundred GeV, and κ/λ on the order of a few percent, m_{χ_1} drops below 10 GeV.

More interesting is the CP-even spectrum. For analytic convenience we consider moderate $\tan\beta$, although the qualitative properties of the figures are also present for lower $\tan\beta$. In the small λ + PQ limit h_1 has a mass

$$(m_{h_1}^2)_{\rm tree} \approx -4v^2\varepsilon^2 + \frac{4v^2\lambda^2}{\tan^2\beta} + \frac{\kappa A_\kappa\mu}{\lambda} + \frac{4\kappa^2\mu^2}{\lambda^2}. \quad (3)$$

at tree level. The heaviest state is strongly down-type, with a mass $m_{h_3}^2 \simeq m_{H_d}^2 \simeq A_\lambda^2$ (where the minimization condition for v_d is used), and the middle state is SM-like.

The h_1 mass is also lifted by quantum corrections, and the strong singlet-like nature of h_1 suppresses contributions from all particles running in the loop except Higgs

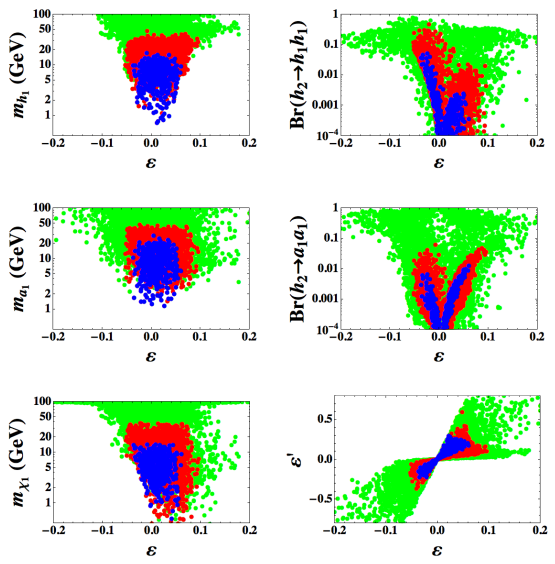

FIG. 1: Masses of h_1 (*top-left*), a_1 (*middle-left*), and χ_1 (*bottom-left*); branching ratios of h_2 into h_1h_1 (*top-right*) and a_1a_1 (*middle-right*), and correlation between ε and ε' (*bottom-right*). Points are taken randomly from the ranges $5 \le \tan\beta \le 50$, $0.05 \le \lambda \le 0.5$, $0.0005 \le \kappa \le 0.05$, $-0.8 \le \varepsilon' \le 0.8$, -40 GeV $\le A_\kappa \le 0$, and 0.1 TeV $\le \mu \le 1$ TeV. (As an illustration, we assume soft squark masses of 1 TeV, slepton masses of 200 GeV, $A_{u,d,e}$ parameters of 750 GeV, and bino, wino and gluino masses of 100, 200 and 660 GeV, respectively, for all numerical analyses in this letter.) Green points cover the whole scan range, red points correspond to $\lambda < 0.30$, $\kappa/\lambda < 0.05$ and $\mu < 400$ GeV, and blue points correspond to $\lambda < 0.15$, $\kappa/\lambda < 0.03$ and $\mu < 250$ GeV.

bosons and Higgsinos. Setting $\varepsilon \to 0$ for these loop diagrams, we find an uplifted singlet mass in the $\overline{MS}$ scheme

$$\Delta m_{h_1}^2 \approx \frac{\lambda^2\mu^2}{2\pi^2} \log \frac{\mu^2 \tan\beta^3}{m_Z^2}. \qquad (4)$$

Fixing all other parameters, the upper bound on $m_{h_1}^2$ is achieved for $\varepsilon \to 0$ and is lowered to about or below 10 GeV in the small λ + PQ limit.

On the other hand, increasing ε rapidly decreases m_{h_1}. Vacuum stability (*i.e.*, $(m_{h_1}^2)_{\rm tree} + \Delta m_{h_1}^2 \ge 0$) indicates an upper bound on ε^2

$$\varepsilon_{max}^2 \approx \frac{1}{4v^2}\left(\frac{4\lambda^2 v^2}{\tan^2\beta} + \frac{\kappa A_\kappa \mu}{\lambda} + \frac{4\kappa^2\mu^2}{\lambda^2} + \Delta m_{h_1}^2\right). \qquad (5)$$

In the small λ + PQ limit and for natural values of μ, $|\varepsilon_{max}|$ is small. This fact will be relevant for collider constraints discussed below. The right-bottom panel of FIG. 1 also shows that A_λ is usually close to $\mu\tan\beta$ for blue points, so we will take a smaller range of ϵ' in our DM analysis.

The tree-level mixing parameters of the light scalar are

$$S_{1d} \approx \frac{v}{\mu\tan\beta}\left(\lambda + \frac{2\varepsilon\mu}{m_Z}\right), \quad S_{1u} \approx \frac{2v\varepsilon}{m_Z}, \qquad (6)$$

indicating a mostly singlet/down admixture in the limit $\varepsilon \to 0$ and an approximately pure singlet (*i.e.*, $S_{1s} \to 1$) in the further limit of small λ or large $\tan\beta$.

There are three main processes by which present experiments potentially constrain this scenario: (1) decays of the SM-like Higgs h_2 through h_1h_1 and a_1a_1, (2) $\Upsilon(ns)$ decays to γh_1 or γa_1, and (3) flavor physics.

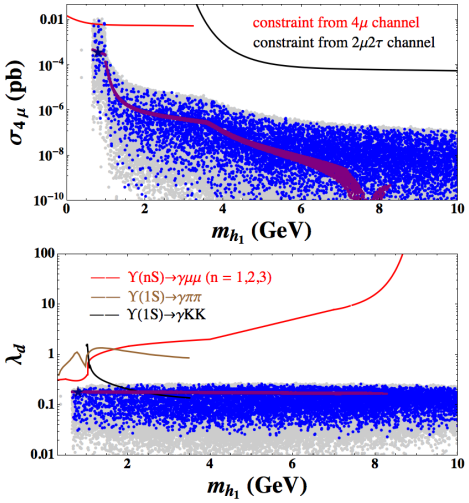

FIG. 2: Constraints from the decays $h_2 \to h_1h_1 \to 4f$ (*top*) and from the decays $\Upsilon \to \gamma h_1(h_1 \to \mu\mu, \pi\pi, KK)$ (*bottom*). $\sigma_{4\mu} \equiv \sigma_{h_2}{\rm Br}(h_2 \to h_1h_1 \to 4\mu)$. To show the constraint from the $2\mu2\tau$ channel on the same plot we convert it into an effective constraint on 4μ by rescaling it with $\frac{{\rm Br}(h_1\to\mu\mu)}{{\rm Br}(h_1\to\tau\tau)}$ (a model-independent quantity). λ_d is a tree-level coupling of the down-type interaction $-\frac{\lambda_d m_{f_d}}{\sqrt{2}v} h_1 \bar{f}_d f_d$. Gray and blue points correspond to the gray and blue points in FIG. 3. Purple bands correspond to the points in the scan of FIG. 4.

Similarly to the light a_1 scenario of [2], relevant constraints may come from the searches for [4, 5]

$$h_2 \to h_1h_1, a_1a_1 \to 4b, 4\tau, 2b2\tau \quad \text{(LEP)},$$
$$h_2 \to h_1h_1, a_1a_1 \to 4\mu, 2\mu2\tau \quad \text{(Tevatron)}.$$

However, in our case the tree-level couplings of h_2 to h_1h_1 and a_1a_1 are suppressed. This can be seen as follows. Since h_1 is strongly singlet-like and h_2 is up-type, the coupling $y_{h_2h_1h_1}$ is (for a complete formula, see [10])

$$y_{h_2h_1h_1} \approx -\frac{\lambda v m_Z \varepsilon}{\sqrt{2}\mu}. \qquad (7)$$

Here we use the mixing parameters at lowest order in ε

$$S_{2d} \approx \cot\beta, \quad S_{2s} \approx -\frac{2\varepsilon v m_Z}{m_Z^2 + \mu^2} \qquad (8)$$

for moderate $\tan\beta$. Similarly, one can find $y_{h_2a_1a_1} = y_{h_2h_1h_1}$ at this order. Both ${\rm Br}(h_2 \to h_1h_1)$ and ${\rm Br}(h_2 \to a_1a_1)$ are thus suppressed by $\lambda\varepsilon \ll 1$, as is shown in the right column of Fig. 1. (Instead, h_2 can dominantly decay into χ_1 and χ_2, while χ_2 dominantly decays into light

Higgs bosons and χ_1. These facts imply rich Higgs phenomenology in the DLH scenario and can dramatically change the strategies of searching for the SM-like and light Higgs bosons at colliders [11].) The asymmetry in $\mathrm{Br}(h_2 \to h_1 h_1)$ w.r.t. ε is caused by an $\mathcal{O}(\varepsilon^2)$ correction with the opposite sign of the term in Eq. (7).

The Tevatron constraints from the search for $h_2 \to h_1 h_1 \to 4f$ are illustrated in the upper panel of FIG. 2. Almost all points survive. Similar limits from LEP are avoided easily for the present parameter values, because m_{h_2} is above the kinematic threshold[1].

Υ physics constrains models with light states through $\Upsilon \to \gamma(h_1, a_1) \to \gamma(\mu\mu, \pi\pi, KK)$. Fig. 2 shows the constraints from searches for these decays on the effective coupling λ_d of the light state to down-type fermions [8, 9]. At tree level, $\lambda_d \approx \frac{v}{\mu}\left(\lambda + \frac{2\varepsilon\mu}{m_Z}\right)$, and the scan points typically approach the constrained region only for $\lambda \gtrsim 0.15$.

B-physics may also add non-trivial constraints with a light a_1 (e.g., see [10]) or h_1, because flavor-violating vertices $b(d,s)(a_1, h_1)$ can be generated at loop level. These vertices, however, depend strongly on the structure of soft breaking parameters (e.g., see [12]). For the input parameters to NMSSMTools used in the scan, the points in the figures are consistent with all B-physics constraints including $B_s \to \mu\mu$, $B_d \to X_s\mu\mu$, $b \to s\gamma$, etc. In addition, though not included in NMSSMTools, we also check the constraints from D meson decays (e.g., $D \to l^+l^-$). Because of the singlet-like nature of h_1 and a_1, D-physics constraints are very weak and can be satisfied easily.

To study the DM physics in the DLH scenario, we perform a second random scan over its parameter region (a narrower region than the one in the first scan). FIG. 3 shows that the χ_1 DM candidate is characterized by a larger spin-independent direct-detection cross section $\sigma_{\rm SI}$, compared with typical supersymmetric scenarios. For certain parameter window, the correct relic density and a large $\sigma_{\rm SI}$ consistent with the CoGeNT and DAMA/LIBRA preferred region [14] can be simultaneously achieved, and the scenario remains consistent with current experimental bounds (particularly from flavor physics and Higgs searches). This has been considered difficult or impossible in supersymmetric models [15–17].

The large $\sigma_{\rm SI}$ is mainly due to the h_1-mediated

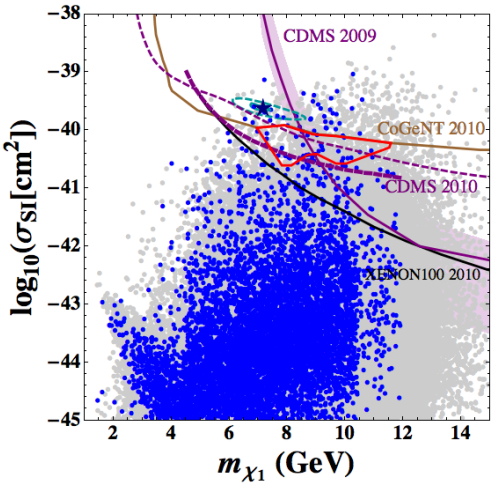

FIG. 3: Cross section of SI direct detection for χ_1. The scan is over all parameters, in the ranges $0.05 \le \lambda \le 0.15$, $0.001 \le \kappa \le 0.005$, $|\varepsilon'| \le 0.25$, $-40 \le A_\kappa \le 0$ GeV, $5 \le \tan\beta \le 50$ and $100 \le \mu \le 250$ GeV. The dark blue (dark) points have a relic density $0.09 \le \Omega h^2 \le 0.13$. The red contour is the CoGeNT favored region presented in [13] and the two blue circles are the most recent interpretations of fitting CoGeNT + DAMA/LIBRA [14]. All contours assume a local density which may be sensitive to the relic density. The purple, brown, and black lines are the limits from CDMS [18], CoGeNT [13], and XENON100 [19], respectively. Most CoGeNT favored regions have a tension with the CDMS constraints. Consistency between the CoGeNT preferred regions and the XENON100 constraints can be achieved within the scintillation-efficiency uncertainties of liquid xenon [14].

$t-$channel scattering $\chi_1 q \to \chi_1 q$, and $\sigma_{\rm SI} \approx$

$$\frac{\left(\left(\frac{\varepsilon}{0.04}\right) + 0.46\left(\frac{\lambda}{0.1}\right)\left(\frac{v}{\mu}\right)\right)^2 \left(\frac{y_{h_1\chi_1\chi_1}}{0.003}\right)^2 10^{-40}\mathrm{cm}^2}{\left(\frac{m_{h_1}}{1\mathrm{GeV}}\right)^4}. \quad (9)$$

The $h_1\chi_1\chi_1$ coupling is reduced to $y_{h_1\chi_1\chi_1} \approx -\sqrt{2}\kappa$ for a singlino-like χ_1 and singlet-like h_1. The dependence of $\sigma_{\rm SI}$ on $m_{h_1}^{-4}$ is illustrated in the left panels of FIG. 4. For the parameter values given in the caption, the LEP search for $h_2 \to bb$ sets the lower boundary of the contoured region, flavor constraints control the upper-right, vacuum stability sets the upper-left limit, and the upper bound on the relic density controls the left and right limits. The sensitivity to $\tan\beta$ enters mainly via m_{h_1}.

The χ_1 relic density is largely controlled by the a_1-mediated annihilation $\chi_1\chi_1 \to f\bar{f}$, with cross section

$$\sigma_{f\bar{f}} v_{\chi_1} \approx \frac{3|\, y_{a_1\chi_1\chi_1}\, y_{a_1 ff}|^2 (1 - m_f^2/m_{\chi_1}^2)^{1/2}}{32\pi m_{\chi_1}^2 \left(\delta^2 + \left|\frac{\Gamma_{a_1} m_{a_1}}{4m_{\chi_1}^2}\right|^2\right)}, \quad (10)$$

where $y_{a_1\chi_1\chi_1} \approx -i\sqrt{2}\kappa$ and $\delta \equiv \left|\frac{1}{1 - v_{\chi_1}^2/4} - \frac{m_{a_1}^2}{4m_{\chi_1}^2}\right|$, with v_{χ_1} denoting the relative velocity of the two χ_1s.). $\delta_{v_{\chi_1}\to 0}$ reflects the deviation of $2m_{\chi_1}$ from the a_1 resonance. In

[1] The LEP and Tevatron constraints from the channel $h_2 \to a_1 a_1$ are included in NMSSMTools and in our code, respectively. Points are omitted if the limit is violated. Similarly, the constraint from $\Upsilon \to \gamma a_1$ is checked by NMSSMTools, so we present only the limit from $\Upsilon \to \gamma h_1$ in FIG. 2. For the numerical results presented in this letter we incorporate *all* built-in checks in NMSSMTools 2.3.1 (including those from LEP Higgs searches, superpartner searches, $g_\mu - 2$, flavor physics, Z-decay, η_b physics, etc.), except the DM relic density. The difference between FIG. 1 and FIG. 3-4 is that in the latter, $\Omega h^2 \le 0.13$ is also required.

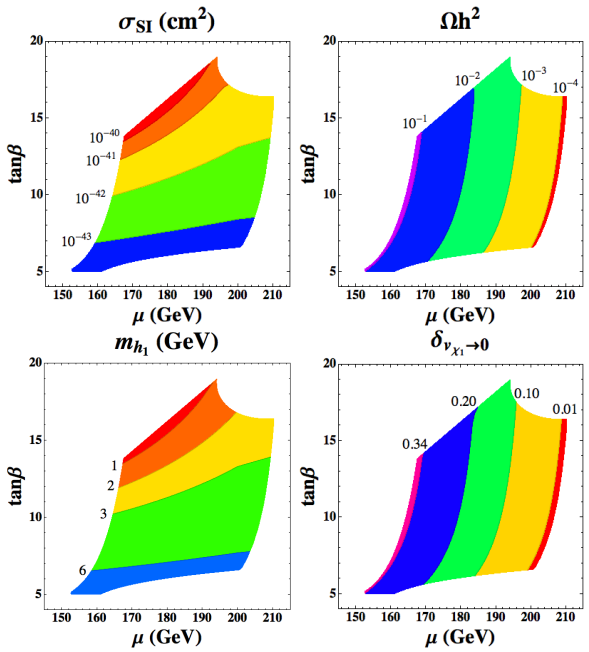

FIG. 4: Contours of $\sigma_{\rm SI}$ (*top-left*), Ωh^2 (*top-right*), m_{h_1} (*left-bottom*) and $\delta_{v_{\chi_1}\to 0}$ (*right-bottom*) on the $\mu - \tan\beta$ plane, with $\lambda = 0.12$, $\kappa = 2.7\times 10^{-3}$, $\varepsilon' = 0.15$ and $A_\kappa = -24$ GeV.

the typical case $m_{a_1} > 2m_{\chi_1} > 2m_b$, the relic density is

$$\Omega h^2 \approx \frac{0.1\left(\frac{m_{a_1}}{15\text{GeV}}\right)\left(\frac{\Gamma_{a_1}}{10^{-5}\text{GeV}}\right)\left(\frac{0.003}{y_{a_1\chi_1\chi_1}}\right)^2\left(\frac{0.1}{\lambda}\frac{\mu}{v}\right)^2}{\text{erfc}\left(\frac{2m_{\chi_1}}{m_{a_1}}\sqrt{x_f\delta_{v_{\chi_1}\to 0}}\right)/\text{erfc}\,(2.2)} \quad (11)$$

where $x_f = m_{\chi_1}/T_f$ is the freeze-out point. As a measure of thermal suppression, $\delta_{v_{\chi_1}\to 0}$ enters the complementary error function obtained from the integral over the Boltzmann distribution. The inverse dependence of Ωh^2 on $\delta_{v_{\chi_1}\to 0}$ is shown in the right panels of FIG. 4. Its sensitivity to μ is mainly through $\delta_{v_{\chi_1}\to 0}$, as $m_{\chi_1}/m_{a_1} \propto \sqrt{\mu}$ for $\tan\beta \gtrsim 5$. To achieve the correct relic density requires $\delta_{v_{\chi_1}\to 0} \approx 0.30 - 0.35$, which implies $A_\kappa \approx -3.5 m_{\chi_1}$, with a tuning range about $\pm 0.1 m_{\chi_1}$. We emphasize that this process does not generate an antiproton or γ-ray flux in tension with existing cosmic-ray data because of the Breit-Wigner suppression effect today [20].

Finally, a benchmark point corresponding to the stars in FIG. 2 and FIG. 3 is given in Table I. We would like to point out that the chosen set of parameters in the squark, slepton and gaugino sectors in this letter provide a realization of the DLH scenario. Changing them can change the details of the phenomenology, but the basic features will remain intact. We reserve an extended phenomenological analysis of this scenario for future work.

λ	$\kappa(10^{-3})$	$A_\lambda(10^3)$	A_κ	μ	$\tan\beta$	m_{h_1}
0.1205	2.720	2.661	-24.03	168.0	13.77	0.811
m_{a_1}	m_{χ_1}	m_{h_2}	Brhh	Braa	Ωh^2	$\sigma_{\rm SI}(10^{-40})$
16.7	7.20	116	0.158%	0.310%	0.112	2.34

TABLE I: Benchmark point. We use the units cm^2 for $\sigma_{\rm SI}$ and GeV for dimensionful input parameters, and denote $\text{Br}(h_2 \to h_1 h_1)$ as Brhh and $\text{Br}(h_2 \to a_1 a_1)$ as Braa. Soft sfermion and gaugino parameters are as given in the caption of FIG. 1.

Acknowledgments

Work at ANL is supported in part by the U.S. DOE Grant DE-AC02-06CH11357. Work at EFI is supported in part by the DOE Grant DE-FG02- 90ER40560. T.L. is supported by the Fermi-McCormick Fellowship and the DOE Grant DE-FG02-91ER40618 at U. California, Santa Barbara. L.-T.W. is supported by the NSF under grant PHY-0756966 and the DOE OJI award under grant DE-FG02-90ER40542. H.Z. is supported by the National NSF of China under Grants 10975004 and the CSC File No. 2009601282. T.L. thanks Princeton U. and Shanghai Jiaotong U. for hospitality during preparation of this work. T.L. thanks Z.-W. Liu for useful discussions.

[1] B. A. Dobrescu *et al.*, Phys. Rev. D **63**, 075003 (2001)
[2] R. Dermisek *et al.*, Phys. Rev. Lett. **95**, 041801 (2005).
[3] P. Ciafaloni *et al.*, Phys. Lett. B **404**, 83 (1997); D. J. Miller *et al.*, arXiv:hep-ph/0501139.
[4] S. Schael *et al.* [ALEPH, DELPHI, L3, and OPAL Collaborations], Eur. Phys. J. C **47**, 547 (2006); S. Schael *et al.* [ALEPH Collaboration], JHEP **1005**, 049 (2010).
[5] V. M. Abazov *et al.* [D0 Collaboration], Phys. Rev. Lett. **103**, 061801 (2009).
[6] U. Ellwanger *et al.*, JHEP **0502**, 066 (2005)
[7] G. Belanger *et al.*, arXiv:1004.1092 [hep-ph].
[8] D. McKeen, Phys. Rev. D **79**, 114001 (2009); Phys. Rev. D **79**, 015007 (2009).
[9] B. Aubert *et al.* [BABAR Collaboration], Phys. Rev. Lett. **103**, 081803 (2009).
[10] U. Ellwanger *et al.*, arXiv:0910.1785 [hep-ph].
[11] P. Draper *et al.*, in preparation.
[12] M. Carena *et al.*, Phys. Rev. D **79**, 075025 (2009).
[13] C. E. Aalseth *et al.* [CoGeNT collaboration], arXiv:1002.4703 [astro-ph.CO].
[14] D. Hooper *et al.*, arXiv:1007.1005 [hep-ph].
[15] D. Feldman *et al.*, Phys. Rev. D **81**, 117701 (2010); E. Kuflik *et al.*, Phys. Rev. D **81**, 111701 (2010); K. J. Bae *et al.*, arXiv:1005.5131 [hep-ph]; J. Cao *et al.*, JHEP **1007**, 044 (2010); D. Das *et al.*, JHEP **1009**, 085 (2010); A. Bottino *et al.*, Phys. Rev. D **67**, 063519 (2003).
[16] A. V. Belikov *et al.*, arXiv:1009.0549 [hep-ph].
[17] J. F. Gunion *et al.*, arXiv:1009.2555 [hep-ph].
[18] Z. Ahmed *et al.* [The CDMS-II Collaboration], Science **327**, 1619 (2010); D. Akerib *et al.* [CDMS Collaboration], arXiv:1010.4290 [astro-ph.CO]; Z. Ahmed *et al.* [CDMS-II Collaboration], arXiv:1011.2482 [astro-ph.CO].
[19] E. Aprile *et al.*, arXiv:1005.0380 [astro-ph.CO].
[20] O. Adriani *et al.* [PAMELA Collaboration], Phys. Rev. Lett. **105**, 121101 (2010); M. Ackermann *et al.* [Fermi LAT Collaboration], arXiv:1008.3999 [astro-ph.HE]; J. Lavalle, arXiv:1007.5253 [astro-ph.HE].